Soft Matter

PAPER

View Article Online
View Journal | View Issue

Cite this: *Soft Matter*, 2025, **21**, 3859

Granular flow of 3D mixtures of soft and hard spheres†

Bo Fan, [ab] Tivadar Pongó, [c] Joshua A. Dijksman, [bd] Jasper van der Gucht [b] and Tamás Börzsönyi *[a]

Received 7th April 2025,
Accepted 8th April 2025

DOI: 10.1039/d5sm00354g

rsc.li/soft-matter-journal

The discharge of granular mixtures composed of hard frictional beads and soft low-friction beads was investigated in a cylindrical silo in experiments and numerical simulations. In the two limits, we find a fill height dependent flow rate for 100% low friction soft grains and a height independent flow rate for 100% hard frictional grains. When mixing the two types of grains, the transition between the two limiting cases occurs rather abruptly. Namely, adding only 20% of hard frictional grains to a sample of low friction soft grains changes the dependence of the flow rate on the discharged mass significantly, *i.e.* causes the slope of the curve to decrease by 50–70%. Our numerical simulations reveal that the main factor leading to the strong change in the flow rate behavior at low hard grain concentration is the high sensitivity of the stress conditions in the orifice region to the mixture composition. Since frictional dissipation can be an important factor influencing the flow rate, we also analyze the frictional properties of our samples in two additional experiments: (i) quasistatic shear tests in a split-bottom shear cell and (ii) drag force measurements on an object moved in the mixture. The mixtures show increasing dissipation as a function of increasing hard grain concentration in both of these measurements, but the increase is rather modest in the low concentration range, thus it does not explain the abrupt change in the silo discharge rate.

1 Introduction

Understanding the flow of granular materials is important for various applications in industry or agriculture. We usually think about a granular material as an assembly of hard frictional grains. The flow properties of such materials are complex and are still widely investigated nowadays. Such materials have a very useful feature: they flow out of a container with a constant rate, independent of the filling height, as it was pointed out in the pioneering works of Huber–Burnand, Hagen and Beverloo[1–4] and was further investigated in more recent investigations focusing on the unique pressure conditions in the orifice region (see *e.g.* ref. 5 and 6). Interestingly, for deformable particles with low surface friction, recent work has shown that this classic perspective does not hold anymore. The flow rate becomes height dependent, similarly to the case of liquids,[7] and for smaller orifice, where clogs occur, the probability of clogging also becomes height dependent.[8,9] Furthermore, for immersed granular materials viscous effects resulting from the background fluid can also change the scaling relation between container flux and opening size.[10]

Hydrogel beads are excellent examples of soft particles with low surface friction. Their use becomes increasingly important in various applications in food industry (delivery of drugs, nutrients or probiotics in the gastronintestinal tract) or in agriculture and water purification (removal of dyes, metal ions, organic pollutants or bacteria) and various biomedical applications.[11–14] The effect of particle softness on the rheology of a granulate has been investigated previously in shear flows numerically,[15–17] and hydrogel beads proved to be very useful to gain experimental insight into the microscopic dynamics by sophisticated noninvasive 3-dimensional (3D) imaging techniques.[18–20] The mechanical response of a mixture of soft and hard grains subjected to compression or shear was also investigated in recent studies.[20–23]

As mentioned above, the discharge of low friction soft particles out of a container is very different from the behavior of hard grains. Experiments in a 2-dimensional system allowed the observation of the flow at the level of individual particles.[8,9,24,25] At small orifice sizes, temporary congestions occur which resolve after some time, unlike the permanent clogs observed for hard

[a] *Institute for Solid State Physics and Optics, HUN-REN Wigner Research Centre for Physics, Budapest H-1525, Hungary. E-mail: borzsonyi.tamas@wigner.hu*
[b] *Physical Chemistry and Soft Matter, Wageningen University & Research, Wageningen 6700 HB, The Netherlands*
[c] *Collective Dynamics Lab, Division of Natural and Applied Sciences, Duke Kunshan University, Kunshan, China*
[d] *Institute of Physics, University of Amsterdam, Amsterdam 1098 XH, The Netherlands*

† Electronic supplementary information (ESI) available. See DOI: https://doi.org/10.1039/d5sm00354g

grains. Both the statistics of the temporary congestions for small orifice (in the intermittent flow regime), as well as the discharge rate for larger orifice (in the continuous flow regime) are filling height dependent. Investigations in a 3D silo also unveiled strong differences in the flow field between the cases of hard grains and low friction soft hydrogel beads[26,27] and a strong dependence of the flow rate on the filling height for the latter.[7] This is related to the fact that for hydrogel beads dynamic arch formation and Janssen screening is less pronounced. As a result of this, for low-friction soft grains (i) the local vertical stress σ_{zz} above the orifice decreases from a higher value, *i.e.* spans a wider range during the discharge process and (ii) the value of σ_{zz} has a stronger impact on the outflow rate than for hard grains.[7]

For a mixture of hard grains and hydrogel beads, a transition is expected to happen as a function of concentration between the two different behaviors described above. Interestingly, in a 2D silo, a recent work showed that adding a small amount (5 or 10%) of hard frictional grains to hydrogel beads strongly changes the flow.[28] By adding only 10% of hard grains the constant flow rate was already recovered. The probability of the formation of clogging arches also strongly changed with the concentration of hard grains in 2D silo experiments.[28–30] In view of the striking behavior of the 2D systems, it is also interesting to test how the flow characteristics of mixtures changes with concentration in 3-dimensional configurations, especially because the nature of force chain propagation and wall effects do not trivially generalize from two to three dimensions.

In the present work, we therefore investigate experimentally the flow of mixtures of hydrogel beads and plastic beads in a 3-D silo, exploring the full range (0–100%) of concentrations. We complement these laboratory experiments by numerical simulations using the discrete element model (DEM). Furthermore, our investigations on silo discharge are complemented with two further experimental tests: (i) quasistatic shearing in a split-bottom shear cell and (ii) measuring the drag force on an object moved horizontally in the granulate.

2 Experimental procedures

For the silo discharge experiments, we used an acrylic cylinder with the inner diameter of D_c = 144 mm and a height of 800 mm with a circular orifice with diameter D in the middle of the silo base (see Fig. 1(a)). The silo base was separated from the cylinder by a gap of about 1 mm, and it was held by two load cells. The container below the silo was also held by a load cell. The sample was filled into the silo manually with a filling rate of about 500 g s^{-1} and then the orifice was opened, and the evolution of both the discharged mass and the basal force was monitored throughout the whole discharge process by reading the signals from the loads cells with a sampling rate of 100 Hz.

In the second experiment, the sample was exposed to shear deformation in a cylindrical split bottom device (see Fig. 1(b)). In this setup, the middle of the sample was slowly rotated with a time period of 13 s, while the outer part was stationary, so the region between them (denoted with red color in Fig. 1(b)) was

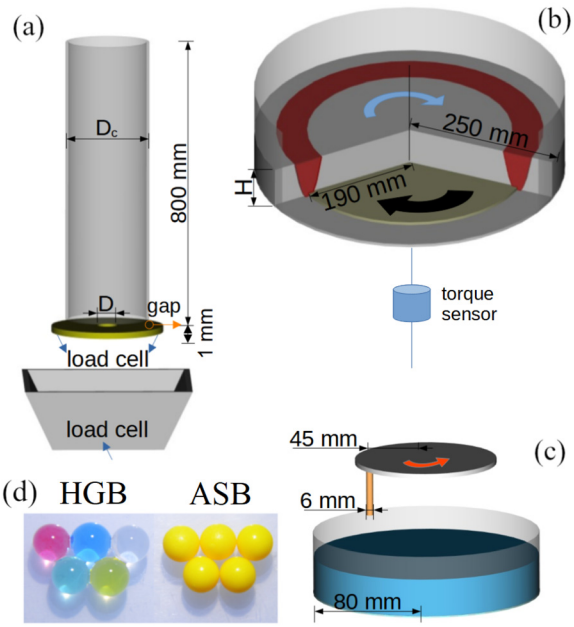

Fig. 1 Experimental setups: (a) silo, (b) cylindrical split-bottom shear cell, (c) rheometer, (d) materials: hydrogel beads (HGB) on the left and airsoft beads (ASB) on the right.

constantly sheared with a typical shear rate of 3 s^{-1}. In order to measure the resistance of the sample against shearing, we measured the torque needed for maintaining stationary rotation of the middle part.

In the third type of experiment, we moved an object horizontally in the mixture and measured the force needed to maintain stationary motion. Two objects were used: an airsoft bead (same as for making the mixtures; glued at the end of a stainless steel needle with diameter of 0.7 mm) or a vertical stainless steel cylinder with the diameter of 6 mm. For each experiment, a 50 mm thick layer of the sample was placed in a cylindrical container with the diameter of 150 mm. Then, the object was immersed at a depth of 22 mm and it was moved using a rheometer (Anton-Paar MCR-501) along a circular trajectory with the radius of 45 mm. The speed of the object was varied in the range of 0.47 cm $s^{-1} \leq v \leq$ 7.54 cm s^{-1}. We can estimate the corresponding shear rate range by dividing the velocity difference of the moving object and the static neighboring grains by the grain size, which results in 0.8 $s^{-1} \leq \dot{\gamma} \leq$ 13 s^{-1}.

In the experiments presented here, we used airsoft beads (ASB) with the diameter of d = 5.95 ± 0.04 mm and hydrogel beads (HGB) with d = 6.4 ± 0.3 mm (for photographs of the beads see Fig. 1(c)). We have investigated 11 samples, spanning the whole concentration range 0–100 wt% (weight percent). The mass density of the two types of grains was identical ρ = 1035 ± 5 kg m^{-3}, as both were slowly sinking/rising in salty water with salt concentrations of 3% or 4%, respectively.

For characterizing the shear resistance as a function of the concentration, we prepared samples with the same volume (V = 10.9 liters), *i.e.* all samples had the same fill height h = 5.6 cm in the shear cell. Since the HGB are deformable, their packing fraction depends on the pressure. For a layer with a

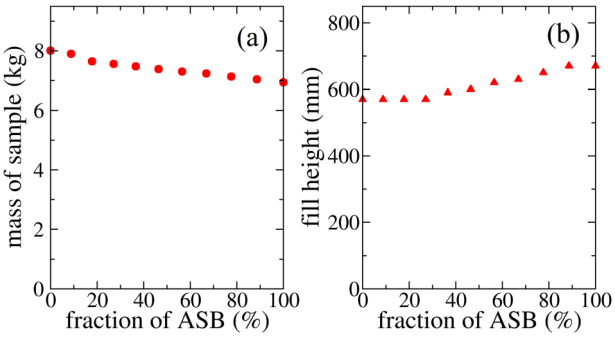

Fig. 2 (a) Mass of the samples (b) fill height in the silo as a function of the ASB concentration.

thickness of h = 5.6 cm, the HGB packing fraction was about 0.7 while that of ASB was measured to be 0.62. Thus, increasing ASB concentration leads to slightly decreasing mass (and density) of the sample. The measured torque was normalized by the mass of the sample. For the silo measurements, the same samples were used. Fig. 2 shows the mass of the samples as well as the fill height in the silo as a function of the ASB concentration.

3 Numerical procedure

We used LIGGGHTS,[31] a Discrete Element Method (DEM) software, to simulate the silo discharge of grain mixtures. The Lagrangian method solves the translational and rotational equation of motions for each particle by using an explicit integration. To calculate the force $\vec{F}_{ij}$ acting between contacting particles i and j, we used the no-slip Hertz–Mindlin model.[32] Note, that we only considered independent pairwise forces, not taking into account the effect of multiple contacts. The force was composed of the nonlinear normal force $\vec{F}_{\mathrm{n},ij}$ and the history dependent tangential force $\vec{F}_{\mathrm{t},ij}$. The latter was constrained by the Coulomb condition $|\vec{F}_{\mathrm{t},ij}| \leq \mu\, |\vec{F}_{\mathrm{n},ij}|$, where μ is the coefficient of friction. The interaction parameters were calculated from the given Young's modulus Y, Poisson's ratio ν and coefficient of restitution e_{n}.

The gravity driven numerical setup included a cylindrical wall and a 1-mm thick bottom mesh wall including the circular orifice. The hard grains were modelled with a Young's modulus of Y_{hard} = 0.5 GPa, the soft ones with Y_{soft} = 300 kPa. The latter value was chosen so that the numerical flow rate results are close to the experimental data. Here we note that this Young's modulus is higher than the usual $\approx$100 kPa, in order to account for the smaller forces due to the lack of a multi-contact interaction.[33] For the hard grains we chose a Young's modulus that is common for plastics, due to this fact their deformation is negligible compared to the soft ones in our system. The Poissons's ratio of each type was set to ν = 0.45, while the coefficient of restitution was e_{n} = 0.9. Following the experiments, the diameter of the hard grains was 5.95 mm and 6.4 mm for soft particles. Due to the small degree of polydispersity of the ASB and softness of the hydrogel beads, we did not implement polydispersity in the numerical system. The mass density of the particles was ρ = 1030 kg m^{-3}. The friction between two hard grains was set to $\mu_{\mathrm{hard-hard}}$ = 0.4, between two soft grains $\mu_{\mathrm{soft-soft}}$ = 0.03, between the two different types it was $\mu_{\mathrm{hard-soft}}$ = 0.1 or $\mu_{\mathrm{hard-soft}}$ = 0.03. The friction coefficient between the wall and hydrogel was set lower, $\mu_{\mathrm{soft-wall}}$ = 0.03, to better match the experimental basal force. The time step of the integration was 10^{-6} s. At the initialization of the simulation, we used Fig. 2(a) for the total mass of the mixtures, to obtain comparable data. The initial packing was created by random insertion of the not overlapping particles, let to settle under gravity (g = 9.8 m s^{-2}). The numerical results presented here were obtained in a system with equivalent size to the experimental one (D_{c} = 144 mm), but we mention that additional simulations were performed with D_{c} = 180 mm, which resulted in the same flow rate, *i.e.* confirmed the absence of finite size effects.

Two main macroscopic measurables were extracted in the simulations, the flow rate and the total force acting on the silo bottom by the grains, similarly to the experiments. Furthermore, we computed the average vertical stress σ_{zz} in the region above the orifice. To do this, firstly we employed a coarse-graining methodology[34,35] that takes the discrete contact force data as input and produces a smooth macroscopic field of the stress tensor. The function used for smoothing the fields was a normalized 3D Gaussian with a standard deviation of w = 1.5 mm, approximately a quarter of the grain diameter. After the continuous field was obtained, the vertical stress was averaged in a cylindrical volume above the supposed free fall arch. A sketch about the position and dimensions of this averaging volume is shown in the inset of Fig. 5(b).

4 Results and discussion

4.1 Silo flow

In the first set of experiments we measured the evolution of the silo flow rate and basal force during the discharge process for all mixtures (see top section of Fig. 3). The flow rate is presented as a function of the mass in the silo for mixtures with different ASB concentration in the top row. Both the flow rate and the mass are normalized by the total mass m_{total} of the sample. The evolution of the basal force F_{b} is shown in the second row. For each sample 3 discharge curves were taken at the orifice sizes of D = 30, 40 and 52 mm. As we see, by increasing the concentration of the ASB we find a gradual change from the hydrogel-like discharge behavior with decreasing flow rate and almost hydrostatic pressure conditions at the bottom of the silo towards a traditional granular-like discharge with constant flow rate and saturating basal force according to the Janssen screening.

The results of the numerical simulations are presented in the bottom section of Fig. 3. We present data for one orifice size (D = 52 mm) and two values of the friction coefficient between the hard and soft grains $\mu_{\mathrm{hard-soft}}$ = 0.1 or 0.03.

In order to quantify how the nature of the silo flow rate changes with the mixture concentration, we take the slope of

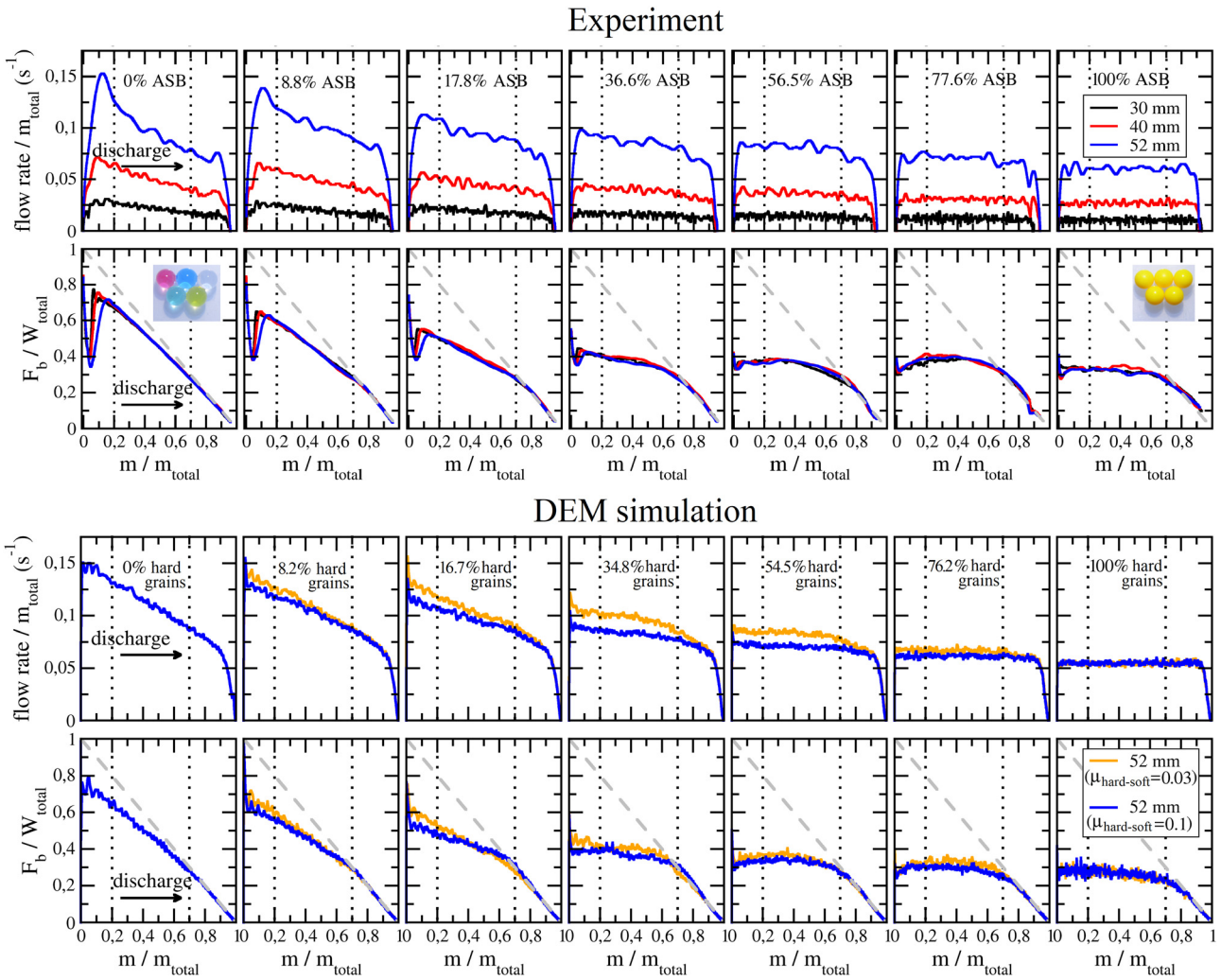

Fig. 3 Silo flow rate and basal force F_b as a function of the discharged mass, normalized by the total mass (m_{total}) or total weight (W_{total}) of the sample in experiments (top section) and DEM simulations (bottom section). The columns correspond to different mixture compositions (0–100 wt% ASB), as indicated on the top. For the basal force the hydrostatic pressure condition is indicated with a grey dashed line as a reference. For the experimental data three discharge curves are shown for each sample corresponding to the orifice sizes of D = 30, 40 and 52 mm, where each curve is a result of the average of two measurements. For the numerical simulations the two curves correspond to different interspecies friction coefficients $\mu_{hard-soft}$ = 0.03 and 0.1. In both cases the orifice size is D = 52 mm and the curve is the result of only one run.

the flow rate curve in the middle part of the discharge process which is free of the initial and final transients, and normalize it with the slope obtained for the pure hydrogel sample. The normalized slope is presented as a function of the percentage of ASB in Fig. 4. As we see, in the experiments the discharge characteristics changes stronger in the beginning of the curve (up to about 20–30% ASB), *i.e.* adding a small amount of hard grains has a strong effect on the behaviour of the sample. But the change is not so dramatic as it was in previous experiments in a 2-dimensional silo,[28] where a constant discharge rate scenario was already reached at 10% ASB. In the present experiments we see a gradual change in the whole concentration range with a stronger dependence up to 20–30% ASB. Note, that the experimental curves obtained for different orifice sizes nicely overlap, when normalized by the flow rate obtained for pure hydrogel for the given orifice.

The data obtained from the numerical simulations shows a similar decreasing trend for the slope of the flow rate, and we see that using a friction coefficient $\mu_{hard-soft}$ = 0.1 results in a better match with the experimental data, than using $\mu_{hard-soft}$ = 0.03. This is similar to our observations in a 2-dimensional system,[28] and probably it is related to the presence of capillary bridges between the grains. Namely, in our earlier work we measured the microscopic friction coefficient of lubricated hard grain–hard grain contacts, and we found that the friction coefficient was much smaller for large normal forces (where capillarity can be neglected) than for small normal forces, where capillary forces are comparable to the normal force.[7] The contact angle of water on a hydrogel surface and on a plastic surface is different, therefore we think that this effect will play a stronger role for ASB–HGB contacts than HGB–HGB contacts, leading to $\mu_{ASB-HGB} > \mu_{HGB-HGB}$. We also mention that

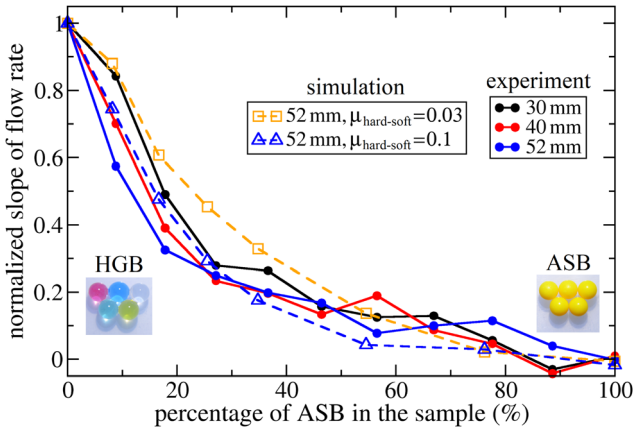

Fig. 4 The slope of flow rate curve obtained by linear fitting between $0.2 < m/m_{\text{total}} < 0.7$ (see the two black dotted lines in Fig. 3) as a function of ASB concentration. The slope is normalized by the slope value obtained for 0% ASB.

in another recent work, a harmonic mean was used to estimate the friction coefficient between hydrogel beads and hard grains, which yields a value closer to the lower coefficient of friction.[21]

4.2 Flow rate response to the vertical stress above the orifice

The numerical simulations allow us to extract further details of the process. Namely, we can study the stress conditions inside the silo, especially in the region above the orifice, which is the most important region determining the discharge rate.[7] In a previous study we have analyzed the differences in the pressure conditions for a system with low friction soft grains and hard frictional grains.[7] When describing the difference between the height dependent discharge rate for hydrogel beads and the height independent discharge rate for hard frictional grains, we found that the very different discharge behavior of these two types of materials is a result of a combination of two different factors. First, during the discharge process the stress above the orifice σ_{zz} changes much more for hydrogel beads than for hard frictional grains, *i.e.* while for hydrogel beads we observe hydrostatic pressure conditions, for the case of hard frictional grains σ_{zz} exhibited a Janssen-like behavior. Second, the discharge rate was much more dependent on the value of σ_{zz} for HGB than for hard frictional grains.[7]

In the present case for the mixtures we have performed a similar analysis, the result of which can be seen in Fig. 5. First, we present the average pressure p_b at the basal plane as well as the local stress σ_{zz} above the orifice as a function of the normalized mass of the granular material above these locations (see Fig. 5(a) and (b)). The local stress σ_{zz} above the orifice was measured in the region indicated with a red box in Fig. 5(b). The curves show a gradual transition from hydrostatic to Janssen-like behavior by increasing the concentration of hard frictional grains. We can quantify this by fitting the data with a Janssen formula:[36–38]

$$p = p_\infty\left(1 - e^{-z/\lambda}\right) = p_\infty\left[1 - \exp\left(-\frac{4(m_{\text{total}} - m)}{\rho_b \pi D_c^2}\Big/\lambda\right)\right]. \quad (1)$$

The fitting parameters λ and p_∞ are shown in Fig. 5(c) as a function of hard grain fraction normalized by the silo diameter D_c and $\rho_b g D_c$, respectively, where ρ_b is the bulk density. As we see, the curve for the local stress σ_{zz} above the orifice changes significantly in the low concentration range, which is clearly represented by the change of the fitting parameters in the Janssen-formula (Fig. 5(b) and (c)). We can also note in Fig. 5(c) that the parameters describing p_b (which is the average pressure calculated from the basal force) change less abruptly in the low concentration range, and this tendency can be described by a simple approximation. For example, taking the case of the characteristic length, it can be expressed as $\lambda = D_c/4\mu_w K$ based on the stress balance model,[37] where μ_w is the particle-wall friction and K is the Janssen constant that characterizes the transmission of vertical to horizontal stress. As a simple model, we assume that both μ_w and K change linearly with the concentration of hard grains between the two limiting values, which are $\mu_w = 0.03$; $K = 1$ at 0% and $\mu_w = 0.4$; $K = 0.484$ at 100%. We estimate a perfectly hydrostatic condition for soft grains resulting in $K = 1$, while for the hard grains K was calculated from the angle of repose of $\phi = 20.5^\circ$ (typical value for spheres[39]) using the $K = (1 - \sin\phi)/(1 + \sin\phi)$[37] formula. This model leads to a characteristic length λ indicated with the dashed line in Fig. 5(c), which fits the parameter corresponding to the basal pressure (blue squares). However, this simple model does not work for the case of σ_{zz}, as it changes much more strongly in the low concentration range (blue circles).

Second, we investigate the effect of σ_{zz} on the discharge rate (Fig. 5(d)). We find that the curves overlap for mixtures with concentrations of up to 25% hard frictional grains, and we only see a gradual decrease of the slope above 25% (Fig. 5(d)). This means that the two factors *i.e.* the slope of stress *vs.* discharged mass curves (blue data in Fig. 5(e)) and the slope of discharge rate *vs.* stress curves (orange data in Fig. 5(e)) contribute unequally to the change in flow rate slope *vs.* concentration curves. The major contribution comes from the dependence of the local stress on the discharged mass, as this quantity changes strongly in the low concentration range (blue data in Fig. 5(e)), while the other quantity (slope of flow rate *vs.* σ_{zz} curves) does not change significantly in the low concentration range.

Finally, in Fig. 5(f) we visualize the slope of the flow rate directly obtained from the simulation data as well as the product of the above described two quantities. As we expect, the two curves nicely overlap. Note, that the quantities in Fig. 5(e) and (f) present data averaged in the $0.2 < m/m_{\text{total}} < 0.7$ interval, which is denoted by a tilde sign.

4.3 Characterization of the frictional properties of the mixtures

Another contributing factor for the change in flow behavior as a function of mixing ratio can be the effective friction characterizing the mixture. This link is especially relevant, noticing that σ_{zz} plays such an important role. It is thus interesting to compare the effect of mixture concentration on the silo discharge and the frictional dissipation during shear flow. In the following we describe the results of our additional experiments focusing on the frictional properties of our mixtures. During the course of silo discharge the sample is subject

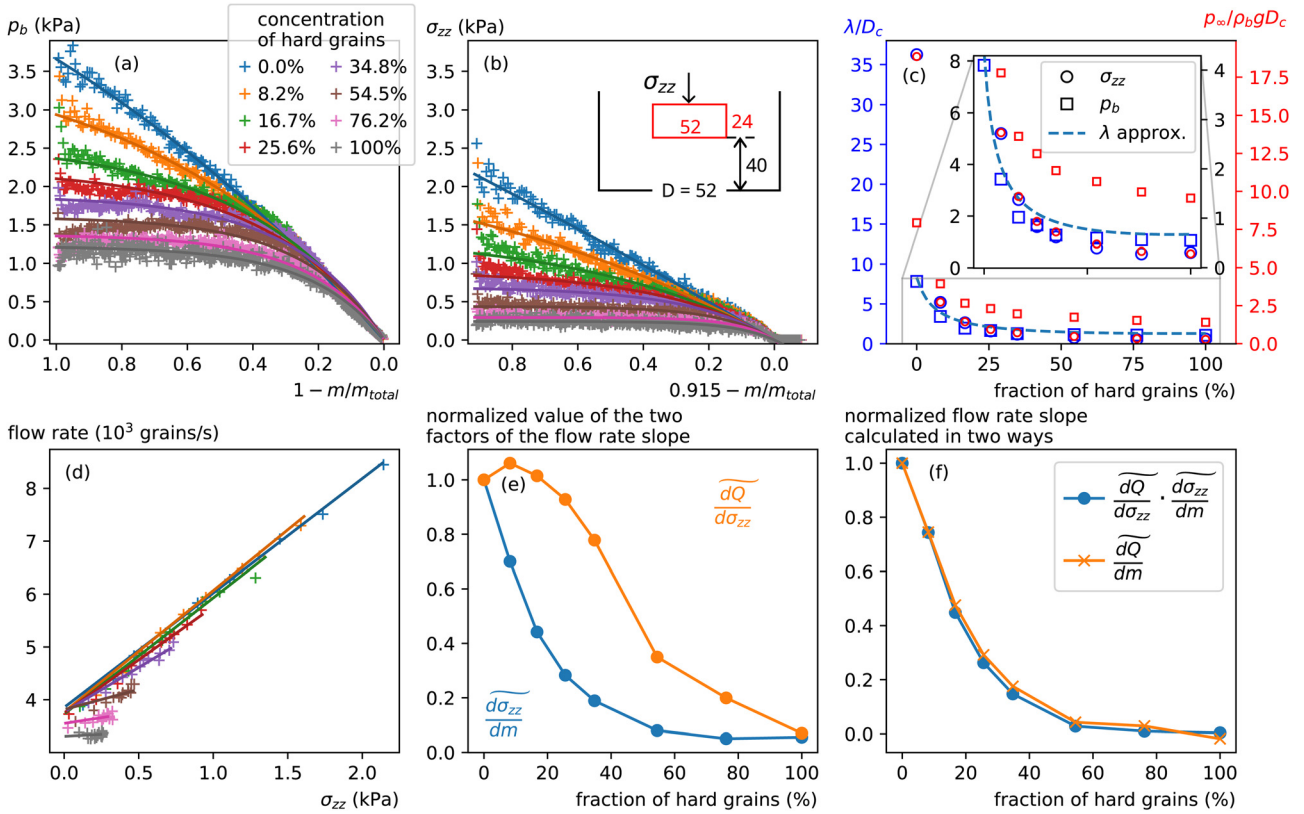

Fig. 5 DEM simulations: (a) average basal pressure p_b and (b) local vertical stress σ_{zz} and as a function of the normalized mass above the relevant location ($1 - m/m_{total}$ or $0.915 - m/m_{total}$) for various values of the concentration (wt%) of hard frictional grains. (c) The characteristic length λ (left y-axis – blue symbols) and saturation pressure p_∞ (right y-axis – red symbols) of the Janssen curves fitted on panels (a) and (b) normalized by the silo diameter D_c and $\rho_b g D_c$, respectively. The dashed line corresponds to a simple approximation of λ as described in the text. The inset displays a magnified version of the indicated region. (d) Flow rate as a function of the local vertical stress σ_{zz}. The red box shows over which domain σ_{zz} was averaged, dimensions are indicated in panel (b) in mm unit. (e) The two contributing factors to the slope of the flow rate *vs.* discharged mass curves: the slope of flow rate *vs.* vertical stress curve and the slope of vertical stress *vs.* discharged mass curve as a function of fraction of hard frictional grains, normalized by their value at 0% concentration. The tilde sign denotes that these quantities were averaged in the $0.2 < m/m_{total} < 0.7$ interval. (f) The normalized slope of the flow rate obtained directly from the simulation data (orange) and from the product of the two factors (blue) from panel (e). All data corresponds to $\mu_{hard-soft} = 0.1$.

to shear deformation within the silo which triggers frictional dissipation.

4.3.1 Shear test in the split-bottom shear cell. In the first experiment, we characterized the resistance of the sample against shearing. The shear resistance was measured in the cylindrical split bottom shear cell, by measuring the torque needed for maintaining stationary rotation of the middle part of the sample, and thereby inducing quasistatic shearing of the material in the shearzone (see red region in Fig. 1(b)). The normalized shear resistance is presented as a function of ASB concentration in Fig. 6. The graph shows two curves, obtained during the first full rotation (13 s), and during the subsequent 6 rotations (78 s), respectively. As we see, the shear torque is larger in the beginning of the experiment (black data points), which is connected to the fact, that during the course of shearing the grains in the shear zone organize themselves into chains along the streamlines.[40] The shear measurement was always started with a random packing, which is harder to shear, and during the course of the experiment the shear resistance slightly decreases due to the above described ordering process. With increasing ASB concentration the shear induced ordering of the samples becomes stronger, since the ASB are more monodisperse than the HGB. Therefore the two curves showing the shear resistance in the disordered state (first 13 s of the measurement) and in the ordered state (following 78 s of the measurement) separate with increasing ASB concentration. Apart from the separation, both curves show the same tendency: a gradual increase of the shear resistance with increasing ASB concentration. Thus, the general trends of the flow rate (Fig. 4) and shear resistance (Fig. 6) are consistent: with increasing hard grain concentration we get stronger resistance against shearing and smaller flow rate in the silo. However, comparing the curves more carefully we find a mismatch: the change in the shear resistance is minor at low ASB concentration and becomes stronger in ASB rich samples, while the tendency is opposite for the silo discharge rate curves, where a small amount of added ASB had a strong influence on the discharge behavior, and in ASB rich samples the flow rate changes less with concentration. This discrepancy is consistent with recent work where we already made a similar observation.[39] Namely, we have investigated the discharge rate of a silo as well as the shear resistance of the samples for ellipsoidal particles as a function of grain shape. We

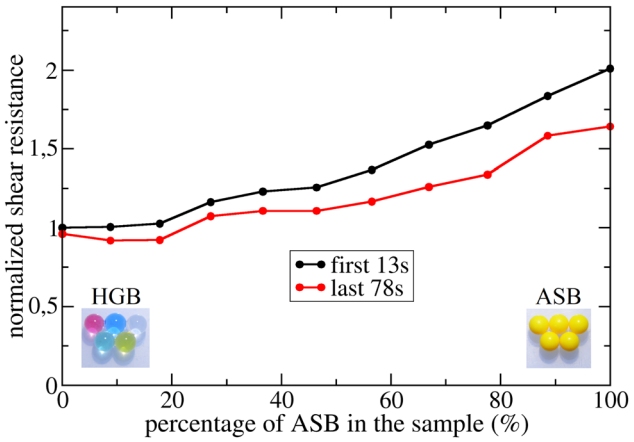

Fig. 6 Shear resistance per mass as a function of the of ASB concentration. The shear resistance data are normalized by the value of the first 13 s of the curve at 0% ASB.

found a non-monotonic behaviour for the discharge rate which was not directly correlated to the shear resistance of the samples. Our current data with the mixtures of ASB and HGB are in line with those observations on ellipsoidal particles.

Another important observation regarding the samples' shear resistance is that even if the microscopic surface friction of common hard grains is more than 1 order of magnitude larger than the value of HGB ($\mu = 0.3$–0.4 *vs.* $\mu = 0.02$–0.03[7]), we see in Fig. 6 that the shear resistance (effective friction) of the sample increases only by about a factor of 2 when going from 0% ASB to 100% ASB. This is perfectly consistent with the result of earlier numerical simulations[41] and work on frictional hydrogel experiments,[42] and again shows the importance of the geometrical origin of the effective friction of a sheared granulate.[43]

We also mention that shearing the mixture might also lead to segregation. If segregation is present, it would also result in a separation of the two curves presented in Fig. 6. As described above, during shearing we have clearly seen the development of ordering, but we did not see signs of segregation during the course of experiments (see ESI† for photographs). In any case, the curve obtained in the first 13 s of the measurement represents the behaviour of the random sample, and has the same trend as the curve obtained at later stages, *i.e.* shear resistance was less sensitive to mixture composition at low ASB concentration than in ASB rich samples.

4.3.2 Drag force on an object moved in the mixture. In our second experiment to characterize the frictional properties of the system, we measured the drag force on an object which was moved horizontally in the sample (see Fig. 1(c)). Here we also tested the rate dependence of the system by performing the experiment at different velocities. In this experiment we used two test objects: an airsoft bead (ASB) and a stainless steel cylinder with the diameter of 6 mm, both immersed at a depth of 22 mm. The velocity of the object was varied in the range of $0.47\ \mathrm{cm\ s^{-1}} \leq v \leq 7.54\ \mathrm{cm\ s^{-1}}$, corresponding to a shear rate range of $0.8\ \mathrm{s^{-1}} \leq \dot{\gamma} \leq 13\ \mathrm{s^{-1}}$.

First, as we see in Fig. 7(a) and (b) the drag force changes with the mixture concentration in a very similar way as the

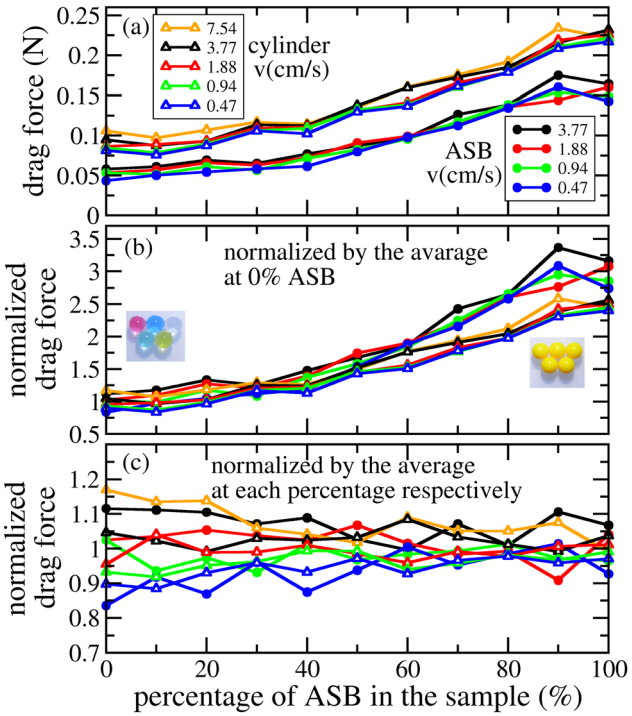

Fig. 7 (a) Drag force on an object (Airsoft bead or vertical cylinder) moved horizontally in the mixture, immersed at a depth of 22 mm. The curves correspond to different velocities v of the object, the values of v are indicated in the figure. (b) and (c) Same data as in panel (a) normalized by the average force at 0% ASB (panel b), and normalized by the average force calculated for each concentration (panel c).

shear torque changed under quasistatic shear in the split bottom shear cell. Generally, the force increases with ASB concentration, and the rate of change is much larger in ASB rich samples than at low ASB concentrations. Thus, similarly to the shear experiments, these data do not provide a reason for the strong change in the slope of the silo discharge rate at low concentration either. The drag force is about 2.5–3 times larger in ASB rich samples than at small concentrations. Naturally, we get a larger drag force for a cylinder than for a single ASB. Second, the shear rate dependence of the drag force appears to be minor, as the data values are very similar even if the shear rate is increased by a factor of 16. In order to better visualize the weak shear rate dependence, we present the data in a normalized form in Fig. 7(c). For high ASB concentration, the data obtained for low and high shear rates are very similar within the uncertainty of the measurement which is about 10%. Decreasing the ASB concentration the curves clearly split up showing a 20–30% difference in the drag force in between the cases with the smallest and largest shear rate. Thus, the drag force on an object in a hydrogel rich sample is increasing with shear rate, similarly to viscous liquids or colloids, but here the magnitude of change is small.

5 Summary

Our measurements on the flow rate of a mixture of hydrogel beads and airsoft (plastic) beads during silo discharge show

that adding hard grains to hydrogel beads strongly changes the discharge behaviour up to the concentration of about 20–30%. Increasing the ASB concentration further has a smaller effect, but the general trend is clear: while ASB rich samples discharge with a constant flow rate (independent of the fill height of the silo), the flow rate of HGB rich samples decreases with decreasing fill height.

Our complementary numerical simulations reveal that the main factor leading to the strong change in the flow rate behavior at low concentration of hard frictional grains is the high sensitivity of the of the stress conditions in the orifice region on the mixture composition. Namely, the slope of the vertical stress above the orifice *vs.* discharged mass curves changes significantly at low concentration of hard frictional grains, while it depends less on the concentration in samples rich in hard frictional grains. Our additional measurements show, that frictional dissipation also increases when increasing the ASB concentration but the dependence is less strong in the low concentration range compared to the trend of the slope of the silo discharge rate.

Author contributions

The laboratory experiments have been carried out by B. Fan and T. Börzsönyi, while the numerical simulations were prepared by T. Pongó. All authors contributed to the writing of the manuscript.

Data availability

Data for this article, including experiments and simulations, and corresponding scripts to process the data are available at Zenodo at **https://doi.org/10.5281/zenodo.13892664**.

Conflicts of interest

There are no conflicts to declare.

Appendix

Since the HGB are inherently wet, our mixtures contain a small amount of water, involving capillary bridges at particle contacts. In order to control of the water content of our samples, in the preparation process we soaked the excess water from the sample with a towel. For the pure ASB sample an additional series of measurements were done to test the effect of added water on the shear resistance of the sample. The resulting data (see Fig. 8) show, that adding water to 6.94 kg of ASB first slightly increases the measured shear resistance, but above 20 grams of added water the curve saturates and no more increase in the shear resistance is observed. The water content of our samples is similar to the ASB sample with 30 g of added water (denoted by a vertical dashed line in Fig. 8). This measurement shows that the data presented above are not especially sensitive to the actual water content.

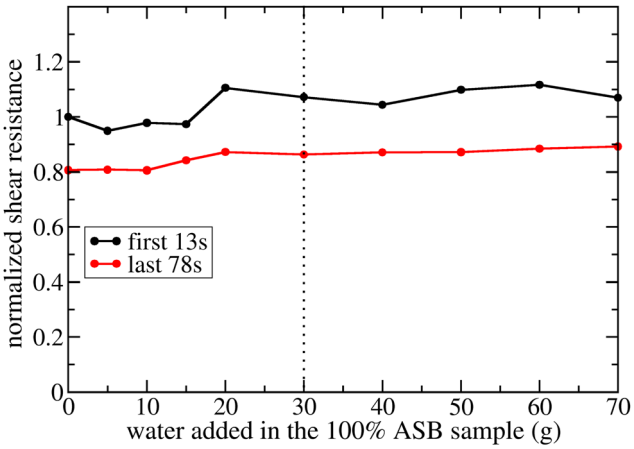

Fig. 8 Shear resistance as a function of added water for 6.94 kg of 100% ASB sample. Data are normalized by the mass of the sample and by the first data point of the curve taken in the first 13 s. The black dotted line indicates the sample with similar moisture content to our mixtures. This sample was used for obtaining the data points in the measurements with 100% ASB sample.

Acknowledgements

The authors acknowledge technical assistance by V. Kenderesi and financial support from the European Union's Horizon 2020 Marie Skłodowska-Curie grant "CALIPER" (no. 812638).

References

1 P. Huber-Burnand, *Ann. Phys.*, 1829, **92**, 316–328.
2 B. P. Tighe and M. Sperl, *Granular Matter*, 2007, **9**, 141–144.
3 W. A. Beverloo, H. A. Leniger and J. Van de Velde, *Chem. Eng. Sci.*, 1961, **15**, 260–269.
4 R. M. Nedderman, U. Tüzün, S. Savage and G. Houlsby, *Chem. Eng. Sci.*, 1982, **37**, 1597.
5 C. Perge, M. Aguirre, J. Grande, P. Cago, L. Pugnaloni, D. Turneau and J.-C. Géminard, *Phys. Rev. E: Stat., Nonlinear, Soft Matter Phys.*, 2012, **85**, 021303.
6 S. M. Rubio-Largo, A. Janda, D. Maza, I. Zuriguel and R. C. Hidalgo, *Phys. Rev. Lett.*, 2015, **114**, 238002.
7 T. Pongó, V. Stiga, J. Török, S. Lévay, B. Szabó, R. Stannarius, R. Hidalgo and T. Börzsönyi, *New J. Phys.*, 2021, **23**, 023001.
8 X. Hong, M. Kohne, M. Morrell, H. Wang and E. R. Weeks, *Phys. Rev. E*, 2017, **96**, 062605.
9 R. Tao, M. Wilson and E. Weeks, *Phys. Rev. E*, 2021, **104**, 044909.
10 Y. Cheng, J. D. Treado, B. F. Lonial, P. Habdas, E. R. Weeks, M. D. Shattuck and C. S. O'Hern, *Soft Matter*, 2022, **18**, 8071–8086.
11 B. Qu and Y. Luo, *Int. J. Biol. Macromol.*, 2020, **152**, 437–448.
12 N. Li and R. Bai, *Sep. Purif. Technol.*, 2005, **42**, 237–247.
13 S. Jain, A. Jain, Y. Gupta and M. Ahirwar, *AAPS PharmSciTech*, 2007, **8**, 56.
14 A. C. Daly, L. Riley, T. Segura and J. A. Burdick, *Nat. Rev. Mater.*, 2020, **5**, 20–43.
15 C. S. Campbell, *J. Fluid Mech.*, 2002, **465**, 261–291.

16 S. Chialvo, J. Sun and S. Sundaresan, *Phys. Rev. E: Stat., Nonlinear, Soft Matter Phys.*, 2012, **85**, 021305.
17 A. Favier de Coulomb, M. Bouzid, P. Claudin, E. Clément and B. Andreotti, *Phys. Rev. Fluids*, 2017, **2**, 102301(R).
18 N. Brodu, J. Dijksman and R. Behringer, *Nat. Commun.*, 2015, **6**, 6361.
19 J. Dijksman, N. Brodu and R. Behringer, *Rev. Sci. Instrum.*, 2017, **88**, 051807.
20 J. Wang, Z. Farmani, J. Dijksman, C. Lübeck, O. Speck and R. Stannarius, *Granular Matter*, 2022, **24**, 103.
21 A. Singh, V. Angelidakis, T. Pöschel and S. Roy, *Soft Matter*, 2024, **20**, 3118.
22 M. Cárdenas-Barrantes, D. Cantor, J. Barés, M. Renouf and E. Azéma, *Phys. Rev. E*, 2020, **102**, 032904.
23 M. Cárdenas-Barrantes, J. Barés, M. Renouf and E. Azéma, *Phys. Rev. E*, 2022, **106**, L022901.
24 A. Ashour, T. Trittel, T. Börzsönyi and R. Stannarius, *Phys. Rev. Fluids*, 2017, **2**, 123302.
25 K. Harth, J. Wang, T. Börzsönyi and R. Stannarius, *Soft Matter*, 2020, **16**, 8013.
26 R. Stannarius, D. Sancho Martinez, T. Finger, E. Somfai and T. Börzsönyi, *Granular Matter*, 2019, **21**, 56.
27 R. Stannarius, D. Sancho Martinez, T. Börzsönyi, M. Bieberle, F. Barthel and U. Hampel, *New J. Phys.*, 2019, **21**, 113054.
28 J. Wang, B. Fan, T. Pongó, K. Harth, T. Trittel, R. Stannarius, M. Illig, T. Börzsönyi and R. Cruz-Hidalgo, *Soft Matter*, 2021, **17**, 4282.
29 S. Alborzi, D. Abrahamyan and S. Hashmi, *Soft Matter*, 2022, **18**, 4127.
30 S. Alborzi, B. Clark and S. Hashmi, *Phys. Rev. E*, 2023, **107**, 024901.
31 C. Kloss, C. Goniva, A. Hager, S. Amberger and S. Pirker, *Prog. Comput. Fluid Dyn.*, 2012, **12**, 140–152.
32 A. Di Renzo and F. P. Di Maio, *Chem. Eng. Sci.*, 2004, **59**, 525–541.
33 N. Brodu, J. A. Dijksman and R. P. Behringer, *Phys. Rev. E: Stat., Nonlinear, Soft Matter Phys.*, 2015, **91**, 032201.
34 I. Goldhirsch, *Granular Matter*, 2010, **12**, 239–252.
35 J. Zhang, R. P. Behringer and I. Goldhirsch, *Progress of Theoretical Physics Supplement*, 2010, vol. 184, pp. 16–30.
36 M. Sperl, *Granular Matter*, 2006, **8**, 59–65.
37 R. M. Nedderman and U. Tuzun, *Statics and Kinematics of Granular Materials*, Cambridge University Press, 1992.
38 Y. Bertho, F. Giorgiutti-Dauphiné and J. Hulin, *Phys. Rev. Lett.*, 2003, **90**, 144301.
39 B. Fan, T. Pongó, R. Hidalgo and T. Börzsönyi, *Phys. Rev. Lett.*, 2024, **133**, 058201.
40 S. Wegner, R. Stannarius, A. Boese, G. Rose, B. Szabó, E. Somfai and T. Börzsönyi, *Soft Matter*, 2014, **10**, 5157–5167.
41 T. Unger, *Phys. Rev. Lett.*, 2007, **98**, 018301.
42 M. Workamp and J. A. Dijksman, *J. Rheol.*, 2019, **63**, 275–283.
43 L. Rothenburg and R. J. Bathurst, *Geotechnique*, 1989, **39**, 601.